J. Phys. B: At. Mol. Opt. Phys. **22** (1989) 951-961. Printed in the UK

Electron scattering from Kr: II. Differential cross sections for the $5s[1\frac{1}{2}]_1$ and $5s'[0\frac{1}{2}]_1$ excitations

A Danjo

Department of Physics, Niigata University, Niigata, 950-21, Japan

Received 27 June 1988, in final form 3 October 1988

Abstract. Differential cross sections have been determined for the $5s[1\frac{1}{2}]_1$ and $5s'[0\frac{1}{2}]_1$ excitations of Kr using a crossed-beam method. The measurements were carried out in the angular range 10-125° at impact energies of 20, 30, 40, 50, 60 and 80 eV. The inelastic scattering cross sections were normalised to the absolute differential cross sections for elastic scattering. Differential magnetic sublevel cross sections have also been determined for the first time at impact energies of 40, 50, 60 and 80 eV and scattering angles of 10°, 15°, 20°, 25° and 30° with the help of previously measured λ parameters.

1. Introduction

Electron-heavy-rare-gas-atom collisions have attracted a great deal of attention in the fields of laser physics and electric gaseous discharge. A systematical study of Kr was undertaken to obtain the electron impact cross sections which are necessary not only for the understanding of scattering problems but also for practical use. The non-*LS*-coupled nature and the complications of the many-electron problem in this system provide a stringent test for theoretical models. The elastic scattering measurements for Kr have been summarised by Danjo (1988). As an extension of this work, inelastic scattering cross sections for Kr have now been measured.

Since the first observations of total scattering cross sections of Kr by Ramsauer (1923) and Ramsauer and Kollath (1929), many experiments have been performed to obtain the total scattering, excitation, ionisation and elastic scattering cross sections. They are summarised in the report of de Heer *et al* (1979). However, there has only been a small amount of work on the differential cross sections for individual excitations of Kr. Lewis *et al* (1975) measured the differential cross sections for the 4p-5s excitation at 50 and 60 eV impact energies. The relative differential cross sections were presented by Delage and Carette (1977) in the electron energy range from 15 to 100 eV. Recently, Trajmar *et al* (1981) have measured absolute differential cross sections for several states of Kr in the 15-100 eV impact energy range. Theoretical calculations have been limited to those of Ganas and Green (1971) who calculated integral cross sections for the 4p-5s optically allowed transitions using a Born approximation with semiempirical distortion corrections. More recently, Meneses *et al* (1985) calculated the differential, integral and momentum transfer cross sections for electron impact excitation of the $5s[1\frac{1}{2}]_1$, $5s'[0\frac{1}{2}]_1$, $5s[1\frac{1}{2}]_2$ and $5s'[0\frac{1}{2}]_0$ states of Kr using first-order many-body theory. They also calculated the scattering parameters λ, $\bar{\chi}$, ε and Δ for the optically allowed transitions.

In the present measurements, electron impact excitation of the $5s[1\frac{1}{2}]_1$ and $5s'[0\frac{1}{2}]_1$ states was studied. The angular range covered is 10-125° and the impact energies are

0953-4075/89/060951+11$02.50

20, 30, 40, 50, 60 and 80 eV. Normalised absolute differential cross sections and integral cross sections have been obtained. The scattering parameters λ, χ and ε were obtained in our previous electron–photon angular correlation experiments on electron impact excitation of Kr $5s[1\frac{1}{2}]_1$ and $5s'[0\frac{1}{2}]_1$ states (Danjo *et al* 1985). Combining the λ parameters with the present differential cross sections, the magnetic sublevel cross sections can be determined for these excitations.

2. Experimental apparatus and procedures

The electron impact spectrometer and the experimental procedures used in the present measurements have been described previously (Nishimura *et al* 1985, Danjo 1988). The Kr beam effused through a capillary array which was crossed with an electron beam at right angles. The energy resolution of the spectrometer was about 60 meV FWHM and the angular resolution was about $\pm 2°$. The impact energy scale was calibrated against the 19.35 eV resonance of He at 90° scattering angle. The true zero scattering angle was determined from the symmetry of scattering around the nominal zero degree angle. The elastically and inelastically scattered electron intensities as functions of energy loss were recorded in a multichannel scaler at a fixed impact energy and scattering angle. A typical energy loss spectrum is shown in figure 1. The $5s[1\frac{1}{2}]_1$ feature is resolved from the $5s[1\frac{1}{2}]_2$ state in the energy loss spectrum, but because of rather poor energy resolution of the present spectrometer the $5s'[0\frac{1}{2}]_1$ feature was not well resolved from the $5s'[0\frac{1}{2}]_0$ state. Hence, the relative intensities of the individual features with respect to the elastic feature were determined by utilising a computer unfolding technique (Trajmar *et al* 1971). The $5s'[0\frac{1}{2}]_0$ feature may contribute to the observed intensity of the $5s'[0\frac{1}{2}]_1$ feature. This contribution is at most 10% at backward scattering angles but negligible at forward scattering angles in the present measurements.

In order to determine the relative differential cross sections of the individual excitations with respect to the elastic scattering from the measured energy loss spectra, the transmission properties of the analyser should be known for the elastically and inelastically scattered electrons. The transmission properties were studied by measuring the secondary-electron energy distributions in the electron impact ionisation of N_2

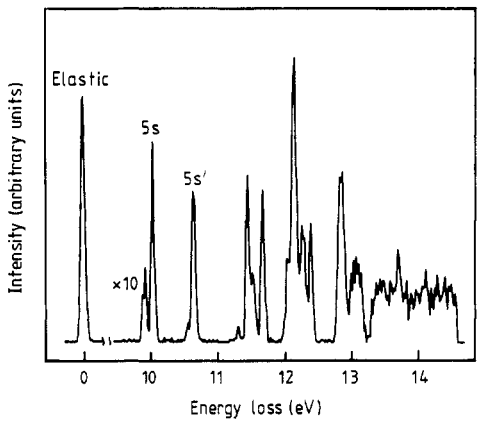

Figure 1. Energy loss spectrum of Kr at 30 eV impact energy and 120° scattering angle.

prior to energy loss spectrum measurements. In the measurements of the energy loss spectrum, for example at 60 eV impact energy, the scattered electrons with kinetic energy from 60 to 46 eV (the corresponding energy loss ranged from 0 to 14 eV) are to be energy analysed. Secondary-electron energy distributions of N_2 were measured in this kinetic energy region at 200 eV impact energy and 60° ejection angle, and the applied voltage to the lens system of the analyser was adjusted so that the measured electron energy distributions reproduced the secondary-electron emission cross sections. The double differential cross sections (DDCS) for electron impact ionisation of N_2 presented by Opal *et al* (1972) were adopted in this procedure. In figure 2, the DDCS of Opal *et al* at 200 eV impact energy and 60° ejection angle are shown along with the recent results of Shyn (1983) and Goruganthu *et al* (1987). It is pointed out that the DDCS of Opal *et al* do not give proper angular distributions especially at both small and large ejection angles (Dubois and Rudd 1978). As shown in figure 2, indeed, their values are systematically larger than the others. However, the energy distribution given by Opal *et al* agrees with the recent revised measurements within the error limits when it is multiplied by a factor of about 0.8. It should be noted that the transmission property can be determined only using the energy distribution of the secondary electrons. Another reason why we adopted the DDCS of Opal *et al* is that none of the other data are presented in a convenient form, i.e. tabulated at sufficient ejected-electron-energy points. The inset in figure 2 shows the measured DDCS at 200 eV impact energy and 60° ejection angle. The present results are normalised at 60 eV to the interpolated value from the data of Opal *et al.* Thus, we can determine the transmission property of the analyser for the energy-loss electrons with about 50 eV kinetic energy and elastically scattered ones with 60 eV. These studies of the transmission property were made at every impact energy studied in the energy loss measurements. The transmission corrections needed for the determination of the relative intensities were less than 10%. Hence, the relative intensities are equal to a good approximation to relative differential cross sections. Absolute inelastic differential cross sections were derived from the relative intensities normalised to the absolute differential cross sections

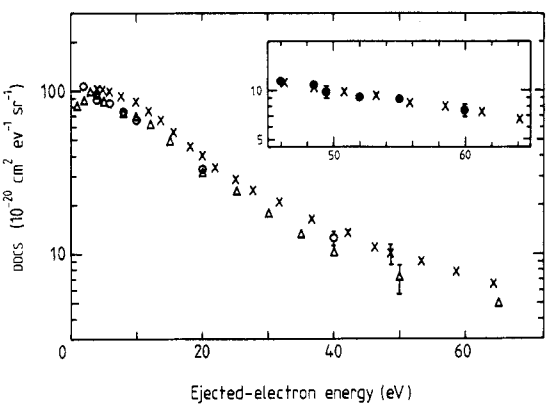

Figure 2. Double-differential cross sections plotted against secondary electron energy at 60° ejection angle for 200 eV e-N_2 collisions. ×, Opal *et al* (1972), some data are omitted and the relative uncertainty is shown at 48.5 eV; △, Shyn (1983), the absolute uncertainty is shown at 50 eV; ○, Goruganthu *et al* (1987), the absolute uncertainty is shown at 40 eV. The inset shows the present DDCS at 200 eV impact energy and 60° ejection angle normalised to those of Opal *et al* at 60 eV; ●, present results; ×, Opal *et al* (1972).

for elastic scattering obtained in previous measurements using the relative flow method (Danjo 1988).

Errors in the determination of the present differential cross sections are attributed to uncertainties in the measurements of the intensity ratios of the $5s[1\frac{1}{2}]_1$ and $5s'[0\frac{1}{2}]_1$ features with respect to the elastic feature and the errors associated with the elastic cross sections. The estimated sources of experimental uncertainties are listed in table 1. The errors in the inelastic to elastic ratio measurements are estimated to be about 25%, which is a quadrature sum of errors in the measurements of the individual intensities and those in the transmission property. In the calibration of the present transmission property, counting statistics are within 10% and the estimated errors due to the long-term fluctuations of electron current and atomic-beam intensity are both about 5%. The DDCS of Opal *et al* are claimed to be accurate within 15% when the primary-electron energy and secondary-electron ejection angle are fixed. This uncertainty is estimated taking into account only the fluctuations of the molecular beam density and the transmission property for the secondary electrons with different kinetic energy, but neglecting the errors in the normalisation. The uncertainties associated with the differential cross sections for elastic scattering have been discussed previously and are taken as 20%. It is estimated that the total error calculated as the square root of the sum of the squares of the individual errors is about 32% for the present differential cross sections. An additional uncertainty of about 20% contributes to the integral cross sections due to the extrapolations.

Table 1. Experimental uncertainties quoted at one standard deviation.

	Source	Uncertainty (%)
A	Intensity ratio	
(i)	Intensity measurements	
	Statistical uncertainty	±10
	Electron current	±5
	Atomic beam intensity	±5
	Quadrature sum	±13
(ii)	Transmission measurements	
	Statistical uncertainty	±10
	Electron current	±5
	Atomic beam intensity	±5
	DDCS	±15[(a)]
	Transmission correction	±10
	Quadrature sum	±22
B	Elastic differential cross section	±20
C	Total uncertainty	±32
(a)	Relative uncertainty (Opal *et al* 1972)	

3. Results and discussion

3.1. Differential cross sections

Absolute differential cross sections for inelastic scattering of the $5s[1\frac{1}{2}]_1$ and $5s'[0\frac{1}{2}]_1$ excitations were obtained in the energy range from 20 to 80 eV. They are given in

Table 2. Differential cross section for the $5s[1\frac{1}{2}]_1$ excitation (in units of 10^{-19} cm^2 sr^{-1}). The integral cross section σ_1 is given in the last row (in units of 10^{-19} cm^2).

Scattering angle (deg)	Incident electron energy (eV)					
	20	30	40	50	60	80
10	138	491	536	611	707	389
15	89	200	203	182	190	82
20	50	87	79	58	57	27
25	32	53	42	31	28	17
30	25	37	30	25	19	13
40	19	21	15	13	9.2	3.0
50	15	13	6.5	4.0	2.4	0.56
60	12	6.3	2.5	1.7	1.1	0.94
70	9.1	3.6	1.0	0.81	1.7	1.2
80	6.3	2.5	1.1	1.1	1.6	0.96
90	4.2	2.3	1.2	1.2	1.2	0.44
100	4.0	2.5	1.4	1.1	0.46	0.11
110	4.6	2.0	0.91	0.68	0.27	0.086
120	7.8	1.6	0.67	0.41	0.16	0.13
125	7.9	1.4	0.57	0.20	0.096	
σ_1	156	221	209	211	211	153

Table 3. Differential cross section for the $5s'[0\frac{1}{2}]_1$ excitation (in units of 10^{-19} cm^2 sr^{-1}). The integral cross section σ_1 is given in the last row (in units of 10^{-19} cm^2).

Scattering angle (deg)	Incident electron energy (eV)					
	20	30	40	50	60	80
10	91	352	425	505	593	353
15	58	144	173	146	154	78
20	39	77	66	47	49	25
25	25	50	36	28	23	14
30	18	29	28	20	15	9.9
40	14	19	13	11	8.6	3.6
50	11	10	6.4	3.7	1.9	0.66
60	9.9	5.2	2.3	1.7	1.0	0.68
70	6.8	3.2	0.90	0.89	1.2	1.1
80	5.4	2.5	0.92	1.1	1.4	1.1
90	4.0	1.9	1.0	1.1	1.0	0.48
100	3.7	2.4	1.3	1.1	0.31	0.070
110	4.4	2.2	0.76	0.55	0.18	0.052
120	6.6	1.9	0.56	0.38	0.13	0.11
125	7.4	1.5	0.49	0.21	0.093	—
σ_1	124	173	175	174	182	118

tables 2 and 3. The differential cross sections for the optically allowed $5s[1\frac{1}{2}]_1$ and $5s'[0\frac{1}{2}]_1$ excitations are usually largest at all energies. Figure 3 shows the present results for the $5s[1\frac{1}{2}]_1$ excitation at several electron energies. They show considerable forward peaked angular distributions especially at high impact energies. Similar angular behaviour is observed also for the optically allowed $5s'[0\frac{1}{2}]_1$ excitation. In the present angular distribution, a minimum is found which shifts toward smaller scattering angles with increasing impact energy. According to Kim *et al* (1968), the generalised oscillator strengths for the $5s[1\frac{1}{2}]_1$ excitation of Kr have a minimum at $(Ka_0)^2 \simeq 0.9$, where a_0 is the Bohr radius and K is the momentum transfer. The experimental generalised oscillator strengths derived from the measured cross sections for the $5s[1\frac{1}{2}]_1$ excitation of Kr at 80 eV impact energy have two minima at $(Ka_0)^2 \simeq 1$ and ~ 4.5. These minima in the generalised oscillator strengths correspond to the shoulder at 25° scattering angle and the minimum at 50° respectively in the differential cross sections. Further discussion is not possible because of rather poor statistics in the present measurements.

In figure 4, the present results at 20 eV impact energy are compared with the earlier experimental and theoretical ones. There is good agreement in the angular distribution of the $5s[1\frac{1}{2}]_1$ excitation between the present results and those of Trajmar *et al* (1981). Also, in magnitude, they agree within error limits though the present results are smaller by about 30–40% at the forward scattering angles. This disagreement could partly

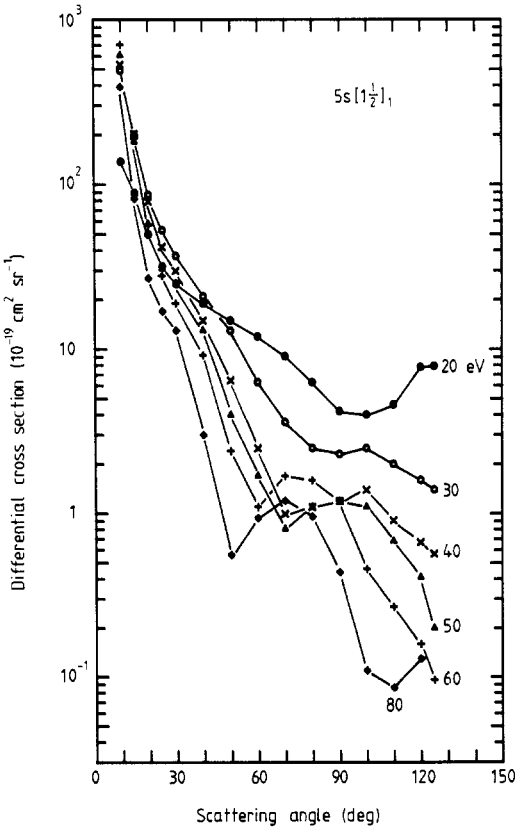

Figure 3. Differential cross sections for the excitation of the $5s[1\frac{1}{2}]_1$ state at 20–80 eV impact energies.

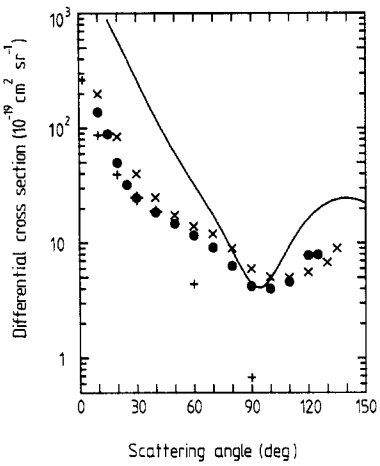

Figure 4. Differential cross sections for the excitation of the $5s[1\frac{1}{2}]_1$ state at 20 eV impact energy. ●, present results; ×, Trajmar *et al* (1981); +, Delage and Carette (1977) (normalised to the present data at 30°). The full curve represents the calculated results of Meneses *et al* (1985).

come from the ambiguities in the transmission property. However, it should be noted that the uncertainties associated with the transmission property, as noted in the previous section, are essentially independent of the scattering angle. The relative measurements of Delage and Carette (1977) normalised to the present data at 30° scattering angle show a steeper angular dependence than the present results. The theoretical calculation of Meneses *et al* (1985) using first-order many-body theory gives much higher cross sections than the present results at both forward and backward scattering angles. In figure 5, the angular distributions for the $5s[1\frac{1}{2}]_1$ excitations at 50 eV impact energy are in reasonable agreement with those of Trajmar *et al.* The data of Delage and Carette normalised to the present result at 30° scattering angle agree with the present angular distribution. At the impact energy of 50 eV, the agreement between the calculations of Meneses *et al* and the present results is improved. The theoretical curve is inside the experimental error in the angular range from 30° to 100°, though substantial differences still exist at forward and backward scattering angles.

3.2. Integral cross sections

In order to obtain the integral cross section, it is necessary to extrapolate the experimental data to 0° and 180° scattering angles. However, it is rather arbitrary when we do not know how to do the extrapolation accurately. We adopted the method used by Trajmar *et al* (1981). The extrapolation to 0° was aided by theoretical predictions and experience with other rare gases. In extrapolating to 180°, we continued the tendency of the curves from 120° to 125° smoothly and from there to 180° the cross section was taken to be constant. As described in Trajmar *et al* (1981), this is for the following reasons: (1) the differential cross sections for the optically allowed transitions are small at large angles and do not contribute much to the integral cross sections, (2) the contribution from the constant cross section can be easily replaced by more precise values when they become available, and (3) the present results can be directly compared with those of Trajmar *et al.* The results for the $5s[1\frac{1}{2}]_1$ and $5s'[0\frac{1}{2}]_1$ excitations are presented in tables 2 and 3.

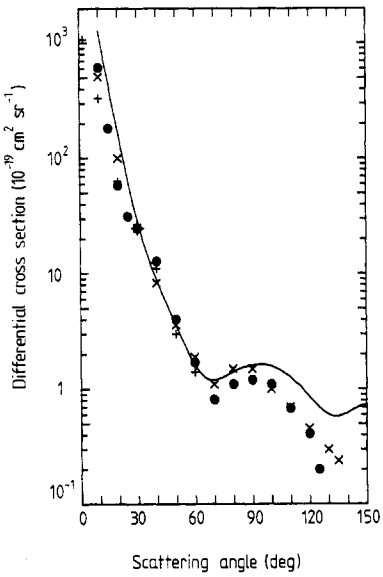

Figure 5. Differential cross sections for the excitation of the $5s[1\frac{1}{2}]_1$ state at 50 eV impact energy. ●, present results; ×, Trajmar *et al* (1981); +, Delage and Carette (1977) (normalised to the present data at 30°). The full curve represents the calculated results of Meneses *et al* (1985).

In figure 6, integral cross sections for the $5s[1\frac{1}{2}]_1$ excitation are shown with the experimental results of Trajmar *et al* (1981) and the theoretical calculations of Ganas and Green (1971) and Meneses *et al* (1985). The present results are in good agreement with those of Trajmar *et al* except at 20 eV impact energy, where the present result is about 30% smaller than the latter though both data are within mutual error bars. The theoretical calculations of Ganas and Green using the Born approximation with a distortion correction can fairly well predict the experimental data at impact energies below 60 eV with larger values at higher impact energies. The calculations by Meneses

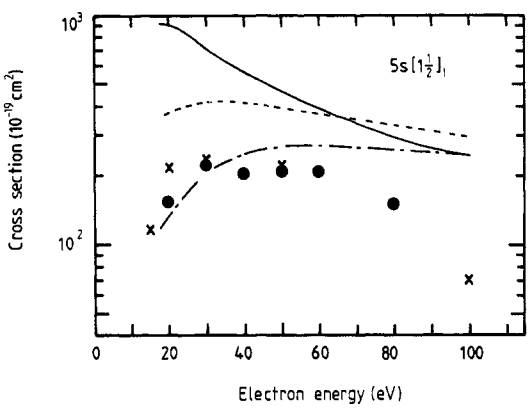

Figure 6. Integral cross sections for the $5s[1\frac{1}{2}]_1$ excitation. ●, present results; ×, Trajmar *et al* (1981); the full curve represents the calculated results of Meneses *et al* (1985). The broken and chain curves represent the calculated results of Ganas and Green (1971) obtained using the Born approximation and applying the distortion correction, respectively.

Table 4. λ parameters and magnetic sublevel cross sections (in units of 10^{-19} cm^2 sr^{-1}).

	40 eV				50 eV				60 eV				80 eV			
θ	σ	λ	σ_0	$2\sigma_1$	σ	λ	σ_0	$2\sigma_1$	σ	λ	σ_0	$2\sigma_1$	σ	λ	σ_0	$2\sigma_1$
								$5s[1\frac{1}{2}]_1$								
10	536	0.19	102	434	611	0.15	92	519	707	0.13	92	615	389	0.10	39	347
15	203	0.34	69	134	182	0.12	22	160	190	0.15	29	161	82	0.26	21	61
20	79	0.36	28	51	58	0.24	14	44	57	0.30	17	40	27	0.74	20	7.0
25	42	0.66	28	14	31	0.64	20	11	28	0.62	17	11	17	0.69	12	5.3
30	30	0.82	25	5.4	25	0.76	19	6.0	19	0.73	14	5.1	13	0.74	9.6	3.4
								$5s'[0^1_2]_1$								
10	425	0.24	102	323	505	0.23	116	389	593	0.13	77	516	353	0.15	53	300
15	173	0.30	52	121	146	0.22	32	114	154	0.24	37	117	78	0.19	15	63
20	66	0.36	24	42	47	0.25	12	35	49	0.37	18	31	25	0.81	20	4.8
25	36	0.53	19	17	28	0.68	19	9.0	23	0.65	15	8.1	14	0.70	9.8	4.2
30	28	0.73	20	7.6	20	0.67	13	6.6	15	0.74	11	3.9	9.9	0.75	7.4	2.5

et al give considerably higher values than the present results. The integral cross sections for the $5s'[0_2^1]_1$ excitation again agree well with the results of Trajmar *et al* except at 20 eV impact energy where the situation is the same as for the $5s[1_2^1]_1$ excitation. The calculations of Meneses *et al* are much higher than the experimental data as in the case of $5s[1_2^1]_1$ excitation.

3.3. Magnetic sublevel cross sections

The correlation parameters λ, χ and ε for the Kr $5s[1_2^1]_1$ and $5s'[0_2^1]_1$ excitations have been determined taking into account the spin-orbit interaction effect in our previous angular correlation experiments at impact energies from 40 to 80 eV and at electron scattering angles from 5° to 30° (Danjo *et al* 1985). Using the parameter λ and the present results, we can obtain the differential magnetic sublevel cross sections for these excitations. The differential cross section σ_0 for the $m=0$ magnetic sublevel and σ_1 for the $m=1$ sublevel of the $J=1$ state are related to the measured differential cross section $(d\sigma/d\Omega)$ as follows:

$$\sigma_0 = \lambda \, d\sigma/d\Omega$$

$$\sigma_1 = \tfrac{1}{2}(1-\lambda)\, d\sigma/d\Omega.$$

The magnetic sublevel cross sections σ_0 and σ_1 are derived at 40, 50, 60 and 80 eV impact energies, and 10, 15, 20, 25 and 30° scattering angles. They are listed in table 4 together with the corresponding λ parameters. In figure 7, the magnetic sublevel cross sections are shown for the excitation of the $5s[1_2^1]_1$ state at 50 eV impact energy together with the calculated results of Meneses *et al* (1985). The angular distribution for σ_1 ($2\sigma_1$ is plotted in the figure) shows a strong forward peaking and a rapid decrease

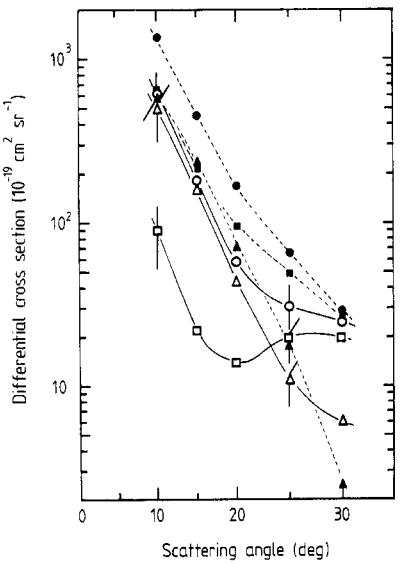

Figure 7. Differential cross sections for magnetic sublevels of the $5s[1_2^1]_1$ excitation at 50 eV impact energy. Present results: ○, σ; □, σ_0; Δ, $2\sigma_1$. Calculation of Meneses *et al* (1985): ●, σ; ■, σ_0; ▲, $2\sigma_1$. The full and broken curves are drawn through the points to guide the eye. Absolute uncertainties are shown at the scattering angles of 10° and 25° (quadrature sum of errors associated with σ and λ).

with the increase of the scattering angle. On the other hand, the differential cross section σ_0 becomes flat at around 15-30° scattering angle also showing a forward peaking. The cross section σ_0 is much higher than σ_1 at scattering angles smaller than 20°, while σ_0 becomes dominant at angles larger than 25°. These general features are commonly observed at the other impact energies studied, and the situations is the same for the excitation of the $5s'[0_2^1]_1$ state. The calculations of Meneses *et al* predict the features observed in the present measurements, that is, forward peaking and rapid decrease for σ_1, and also forward peaking but with slower decrease for σ_0. The good agreement between the present results and the calculations for the cross section σ_1 is rather fortuitous when we consider the discrepancies in the total cross section σ and the scattering parameter λ. Indeed, there are substantial differences not only in magnitude but also in the angular behaviour of the differential cross section σ_0. In order to understand the excitation processes in detail, more systematical studies, both experimentally and theoretically, are needed.

References

Danjo A 1988 *J. Phys. B: At. Mol. Opt. Phys.* **21** 3759
Danjo A, Koike T, Kani K, Sugahara H, Takahashi A and Nishimura H 1985 *J. Phys. B: At. Mol. Phys.* **18** L595
de Heer F J, Jansen R H J and van der Kaay 1979 *J. Phys. B: At. Mol. Phys.* **12** 979
Delage A and Carette J D 1977 *Can. J. Phys.* **55** 1835
Dubois R D and Rudd M E 1978 *Phys. Rev.* A **17** 843
Ganas P S and Green A E S 1971 *Phys. Rev.* A **4** 182
Goruganthu R R, Wilson W G and Bonham R A 1987 *Phys. Rev.* A **35** 540
Kim Y-K, Inokuti M, Chamberlain G E and Mielczarek 1968 *Phys. Rev. Lett.* **21** 1146
Lewis B R, Weigold E and Teubner P J O 1975 *J. Phys. B: At. Mol. Phys.* **8** 212
Meneses G D, da Paixao F J and Padial N T 1985 *Phys. Rev.* A **32** 156
Nishimura H, Danjo A and Sugahara H 1985 *J. Phys. Soc. Japan* **54** 1757
Opal C B, Beaty E C and Peterson W K 1972 *At. Data* **4** 209
Ramsauer C 1923 *Ann. Phys., Lpz.* **72** 345
Ramsauer C and Kollath R 1929 *Ann. Phys., Lpz.* **3** 536
Shyn T W 1983 *Phys. Rev.* A **27** 2388
Trajmar S, Cartwright D C and Williams W 1971 *Phys. Rev.* A **4** 1482
Trajmar S, Srivastava S K, Tanaka H, Nishimura H and Cartwright D C 1981 *Phys. Rev.* A **23** 2167